CHAPTER VII

MOLECULAR STRUCTURE INVESTIGATION, SPECTROSCOPIC CHARACTERIZATION AND UV SPECTRAL ANALYSIS OF (2E)-3-(3-BROMO-4METHOXYPHENYL)-1-(PYRIDIN-2-YL) PROP-2-EN-1-ONE A FOOD PRESERVATIVE CHALCONE

Pyridine and its derivatives are used as solvents and preparatory material for the synthesis of insecticides, herbicides, medicines, vitamins, food flavorings, food additives, drugs, rubber chemicals, explosives, disinfectants and adhesives. (2E)-3-(3-Bromo-4methoxyphenyl)-1-(pyridin-2-yl) prop-2-en-1-one (PYR) is a chalcone derivative and it is used as food preservative and drugs. In the synthesis of various biological active compounds, drugs present in diverse vitamins pyridine and its derivatives are used. The pharmacological activity and the potential use of this chalcone rich plant extort as food preservative has been studied [122]. Attempts were made to explore the structural and spectroscopic investigation of this pyridine derivative chalcone. Some of pyridine derivatives show antimicrobial, antifungal, antibacterial and antitumor properties [123-127]. The significant biological applications draw the attention of experimentalist and theorist. The vibrational spectra with quantum chemical computations have been used as effective tools in the functional group analysis of drugs, biological molecules and NLO active compounds.

7.1 MATERIAL SYNTHESIS AND METHODOLOGY

The title compound was obtained by the condensation of 2-acetyl pyridine (1.21 g, 0.01 mol) with 3-bromo-4-methoxybenzaldehyde (2.15 g, 0.01 mol) in 30

ml ethanol, 10 ml of 10% sodium hydroxide solution was added and stirred at 5–10° C for 3 h. The precipitate formed was collected by filtration and purified by re crystallization from ethanol [128]. The IR spectrum of the sample (PYR) was recorded in the region 4000–450 cm^{-1} using a Perkin Elmer Spectrum 1 FT-IR spectrometer equipped with the standard KBr pellet technique. The resolution of the spectrum is 1 cm^{-1}. The FT-Raman spectrum was recorded in the spectral region between 3500 – 100 cm^{-1} using FT-Raman spectrometer. For recording the spectra the laser line at 1064 nm from an ND: YAG laser was used as Raman excitation source. The laser power of the sample was 100 mW and the spectral resolution is around 2.0 cm^{-1}. By employing Gaussian 09 program package all the DFT computation has been performed [71]. Using the NBO 3.1 program all NBO calculations are carried out [94]. Using MOLVIB program suggested by Pulay *et al* , the Normal coordinate analysis gives the potential energy distribution on the basis of which the vibrational modes were assigned [49,72]. Selective scaling of the force field has been performed by SQMFF procedure [73].

7.2 OPTIMIZED GEOMETRY

Becke's three parameter exchange functional [129], in combination with the Lee-Yang-Parr correlation energy functional [130] (B3LYP), was used for geometry optimization. The optimized structure of the molecule is shown in Fig. 7.1. On comparison with the XRD [128] data the bond length, bond angle and dihedral angle are tabulated in Table 7.1.

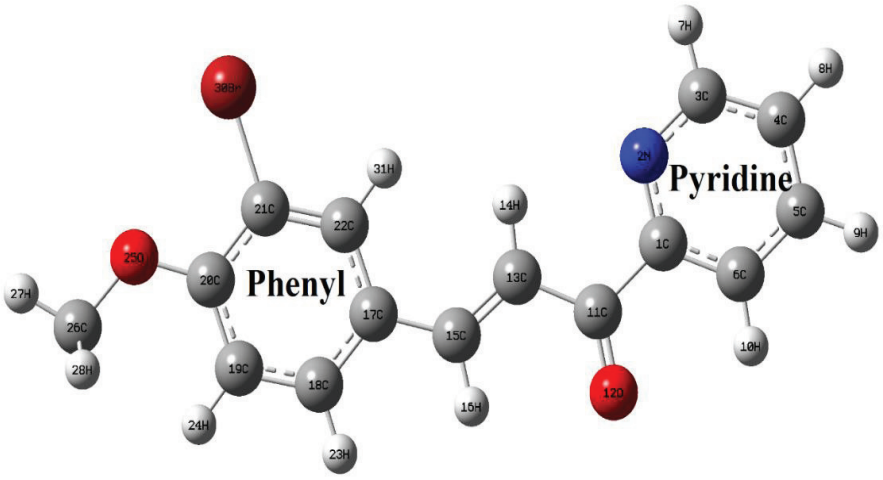

Fig. 7.1 Optimized structure of PYR

The C-C bond distance of the pyridine ring varies in the narrow range 1.390 - 1.400 Å. Due to the fusion of C=O of the propanone group to the carbon atom of the pyridine ring, there is a significant variation of the C_1-C_6 bond length (1.4003 Å) of the pyridine ring. The dihedral angles C_5-C_6-C_1-C_{11} (-179.89˚) and C_{19}-C_{18}-C_{17}-C_{15} (179.99˚) clearly indicate the benzene and the pyridine ring are coplanar with the propanone group. In the pyridine ring, the C-H bond length C_5-H_9 (1.0861Å) slightly increases from the experimental value (0.1381Å) due to the neglect of intermolecular contacts. Inter planar angles (C_{13}-C_{11}-C_1-C_6) and (C_{13}-C_{15}-C_{17}-C_{18}) between the prop-en-one group and the phenyl rings amounts to 178.79 ˚ (pyridine) and -12.85˚ (phenyl ring). The dihedral angle between the mean planes of the pyridine and phenyl ring is 2.8˚. The bond angles N_2-C_1-C_6 (123.03˚) and N_2-C_3-C_4

(123.4˚) are higher than the other bond angles in the pyridine ring. This clearly reveals that the pyridine ring is slightly distorted because of the C=O group substitution which digress from the typical hexagonal angle of (120˚). In the phenyl moiety the electron donating methoxy group is attached to the carbon (C_{20}) atom that increases the bond length C_{19}-C_{20} (1.401 Å) and C_{20}-C_{21} (1.412 Å) compared with C_{21}-C_{22} (1.382 Å) and C_{19}-C_{18} (1.392 Å) at the rest of the substitution. The pyridine moiety along with the carbonyl group (C=O) acts as an electron acceptor at the other end. The charge transfer takes place through the Π-conjugation between the electron donor and acceptor groups. The methoxy group is coplanar with the phenyl ring as exposed by the torsion angle C_{21}-C_{20}-O_{25}-C_{26} (178.15˚).

Table 7.1: Optimized geometrical parameters of PYR in comparison with the XRD data

Bond length	Cal. (Å)	Expt (Å)	Bond angle	Cal. (˚)	Expt. (˚)	Dihedral angle	Calc. (˚)	Expt. (˚)
C_1-N_2	1.343	1.341	N_2-C_1-C_6	123.0	123.1	C_6-C_1-N_2-C_3	-0.81	2.2
C_1-C_6	1.403	1.392	N_2-C_1-C_{11}	118.1	117.8	C_{11}-C_1-N_2- C_3	179.10	-180.0
C_1-C_{11}	1.510	1.504	C_6-C_1-C_{11}	118.8	118.9	N_2-C_1-C_6-C_5	0.09	177.0
N_2-C_3	1.336	1.329	C_1- N_2-C_3	117.7	117.7	N_2-C_1-C_6-H_{10}	179.9	-179.9
C_3-C_4	1.396	1.388	N_2-C_3-C_4	123.4	123.1	C_{11}-C_1-C_6-C_5	179.89	-179.9
C_3-H_7	1.088	0.950	N_2- C_3- H_7	116.1	118.3	C_{11}-C_1-C_6-C_{10}	0.07	0.00
C_{11}-O_{12}	1.230	1.216	C_4-C_5-H_9	120.6	120.6	N_2-C_1-C_{11}-O_{12}	179.58	-179.9
C_{11}-C_{13}	1.474	1.480	C_6-C_5- H_9	120.6	120.5	N_2-C_1-C_{11}-O_{13}	-1.40	0.0006
C_{13}-H_{14}	1.083	0.950	C_1-C_6-C_5	118.5	118.1	C_6-C_1-C_{11}-O_{12}	-0.44	-0.001
C_{13}-C_{15}	1.349	1.344	C_1-C_6-H_{10}	118.7	118.9	C_6-C_1-C_{11}-C_{13}	178.79	180.0
C_{15}-C_{17}	1.457	1.460	C_1-C_{11}-O_{12}	119.3	121.5	C_1-N_2-C_3-C_4	0.71	1.7
C_{17}-C_{18}	1.403	1.391	O_{12}-C_{11}-C_{13}	123.2	122.0	C_1-N_2-C_3-H_7	179.28	180.0
C_{17}-C_{22}	1.410	1.40	C_{11}-C_{13}-H_{14}	116.8	119.4	N_2-C_3-C_4-C_5	0.12	0.0001
C_{18}-C_{19}	1.392	1.383	C_{11}-C_{13}-C_{15}	119.8	120.9	N_2-C_3-C_4-H_8	170.83	-180.0
C_{18}-H_{23}	1.086	0.950	H_{14}-C_{13}-C_{15}	123.3	119.5	H_7-C_3-C_4-C_5	179.89	180.0

Table 7.1 (cont.)

C_{19}-H_{24}	1.083	0.949	C_{13}-C_{15}-H_{16}	116.1	116.7	H_7-C_3-C_4-H_8	0.16	179.8
C_{20}-C_{21}	1.411	1.406	C_{13}-C_{15}-C_{17}	127.8	126.3	C_3-C_4-C_5-C_6	-0.86	178.7
C_{20}-O_{25}	1.352	1.891	H_{16}-C_{15}-C_{17}	115.9	116.9	C_3-C_4-C_5-H_9	179.10	180.0
C_{21}-C_{22}	1.382	1.372	$C_{15}C_{17}$-C_{18}	119.3	119.6	H_8-C_4-C_5-C_6	179.10	180.0
C_{21}-Br_{30}	1.905	1.359	C_{15}-C_{17}-C_{22}	123.0	122.4	H_8-C_4-C_5-H_9	-0.94	179.9
C_{22}-H_{31}	1.083	0.951	C_{18}-C_{17}-C_{22}	117.6	117.8	C_4-C_5-C_6-C_1	0.76	0.05
O_{25}-C_{26}	1.422	1.433	C_{17}-C_{18}-C_{19}	121.7	122.2	O_{12}-C_{11}-C_{13}-H_{14}	177.06	180.0
C_{26}-H_{27}	1.090	0.980	C_{20}-O_{25}-C_{26}	118.6	116.6	O_{12}-C_{11}-C_{13}-C_{15}	5.80	0.001
C_{26}-H_{28}	1.096	0.980	H_{27}-C_{26}-H_{28}	111.4	109.5	C_{18}-C_{19}-C_{20}-O_{25}	178.88	179.99
C_{26}-H_{29}	1.096	0.981	H_{27}-C_{26}-H_{29}	109.3	109.4	C_{19}-C_{20}-C_{21}-Br_{30}	177.55	179.99
			H_{28}-C_{26}-H_{29}	109.3	109.4	C_{21}-C_{20}-O_{25}-C_{26}	178.15	179.99

7.3 NBO ANALYSIS

The NBO analysis can help to identify individual bonds and the energies associated with lone-pair electrons that play an important vital role in the chemical process [131]. NBO analysis is usually applied to study the hybridization, hydrogen bonding as well as hyper conjugative interactions between occupied Lewis type (bonding or lone pair) and unoccupied (anti-bonding or Rydberg) orbitals, which further help in studying inter and intra-molecular interactions among various compounds. These interactions can be quantitatively described by means of the second-order perturbation theory. The strong intra-molecular hyper conjugative interactions of ring π electrons are given by the second order perturbation theory analysis which is presented in Table 7. 2. In general, the interaction energy E (2) associated with i (donor) →j (acceptor) delocalization can be estimated by the following equation [43]

$$\left[E^2\right] = q_i \frac{F^2(i,j)}{\varepsilon_j - \varepsilon_i}$$

where q_i is the donor orbital occupancy, ε_j and ε_i are diagonal elements (orbital energies), and F(i,j) is the off-diagonal Fock matrix element.

Significant amount of hyper conjugative interactions between π (C_{19}-C_{20}) and π* (C_{17}-C_{18}) leads to a stabilization energy of 90.03 kJ/mol. This enhanced π* (C_{19}-C_{20}) NBO further conjugates with π* (C_{17}-C_{18}) resulting in an enormous E(2) energy of 860.89 kJ/mol. Similarly π* (N_2-C_3) conjugate with π* (C_4-C_5) and π* (N_2-C_3) conjugate with π* (C_4-C_5) leading to a stabilization of 60.04 kJ/mol and 546.59 kJ/mol respectively. The lone pair interaction of Lp (3) of Br_{30} with σ* (C_{21}-C_{22}) leads to a stabilization of 45.35 kJ/mol. The ED in the carbonyl C=O antibonding orbital's π* (C_{11}-O_{12}) and σ* (C_{11}-O_{12}) are increased significantly (0.00778e and 0.18187e, respectively) which weakens the bond and the bond length elongates by 0.014 Å. Hyper conjugative interactions of L_P (1) N_2- π* (C_1-C_6), L_P(1) N_2- π* (C_3-C_4), L_P (2) O_{12}- π* (C_1-C_{11}), L_P (2) O_{12}- π* (C_{11}-C_{13}), L_P (2) O_{25}- π* (C_{19} - C_{20}), L_P (3) Br_{30}- σ* (C_{21}-C_{22}) gives rise to enormous amount of charge transfer (39.45, 37.57, 88.24, 81.88, 118.36, 45.35 kJ/mol) which contributes stability to the molecule.

Table 7.2: Donor-acceptor interactions results of PYR followed by Fock matrix in NBO basis

Donor(i)	ED[a] (i) (e)	Energy (i) (a.u)	Acceptor (j)	ED (j) (e)	Energy (j) (a.u)	E(2)[b] (kJ/ mol)	E(j)-E(i)[c] (a.u)	F(i,j)[d] (a.u)
π (C_1-N_2)	1.984	-0.815	π* (C_1-C_6)	0.029	0.571	9.16	1.39	0.04
π (C_1-N_2)	1.984	-0.815	π*(N_2-C_3)	0.015	0.515	4.10	1.33	0.03
π (C_1-C_6)	1.981	-0.714	π* (C_5-C_6)	0.015	0.584	10.25	1.30	0.05
π (C_1-C_6)	1.601	-0.259	π* (N_2-C_3)	0.369	-0.003	73.42	0.26	0.06
π (N_2-C_3)	1.716	-0.299	π* (C_4-C_5)	0.311	0.020	60.04	0.32	0.06
π* (N_2-C_3)	0.015	0.515	π* (C_4-C_5)	0.017	0.575	546.59	0.02	0.08
π (C_{19}-C_{20})	1.662	-0.268	π* (C_{17}-C_{18})	0.372	0.035	90.03	0.30	0.07

Table 7.2 (cont.)

π^* (C_{19}-C_{20})	0.384	0.019	π^* (C_{17}-C_{18})	0.372	0.035	860.89	0.02	0.08
π^* (N_2-C_3)	0.369	-0.003	π^*(C_1-C_6)	0.319	0.027	350.36	0.03	0.07
π(N_2-C_3)	1.716	-0.299	π^*(C_1-C_6)	0.319	0.027	100.08	0.33	0.08
π (C_1-C_6)	1.601	-0.259	π^* (N_2-C_3)	0.369	-0.003	73.42	0.26	0.06
L_P (1) N_2	1.926	-0.355	π^* (C_1-C_6)	0.029	0.571	39.45	0.93	0.08
L_P (1) N_2	1.925	-0.356	π^*(C_3-C_4)	0.025	0.567	37.57	0.92	0.08
L_P (2) O_{12}	1.880	-0.251	π^* (C_1-C_{11})	0.077	0.399	88.24	0.65	0.10
L_P (2) O_{12}	1.880	-0.251	π^* (C_{11}-C_{13})	0.061	0.430	81.88	0.68	0.10
L_P (2) O_{25}	1.840	-0.313	π^*(C_{19}-C_{20})	0.037	0.529	118.36	0.33	0.09
L_P (3) Br_{30}	1.931	-0.287	σ^*(C_{21}-C_{22})	0.347	0.018	45.35	0.30	0.05

b E(2) means energy of hyper conjugative interactions.
c E(j)-E(i) means the energy difference between donor and acceptor i and j Natural bond orbitals.
dF(i,j) is the Fock matrix element between i and j natural bond orbitals.

7.4 VIBRATIONAL ANALYSIS

By adopting Wilson numbering convention the vibrational assignments of the tri-substituted phenyl ring and a mono substituted pyridine ring have been extensively studied [78]. The experimental molecule consists of 31atoms, which undergoes 87 normal modes of vibrations. Vibrational assignments were performed by means of density functional theory with B3LYP/6-31G** basis set. Using normal coordinate analysis a detailed vibrational depiction can be made. The precise assignment to each wave number is given based on the results obtained from PED. Fig. 7.2 shows the observed and simulated FT-IR and FT-Raman spectra. Table 7.3 has been reported the observed and calculated wave numbers together with vibrational assignments, the calculated scaled quantum mechanical frequencies, Infrared and Raman intensities and the normal mode description. The title molecule consists of a benzene ring and a pyridine ring connected by a propanone group.

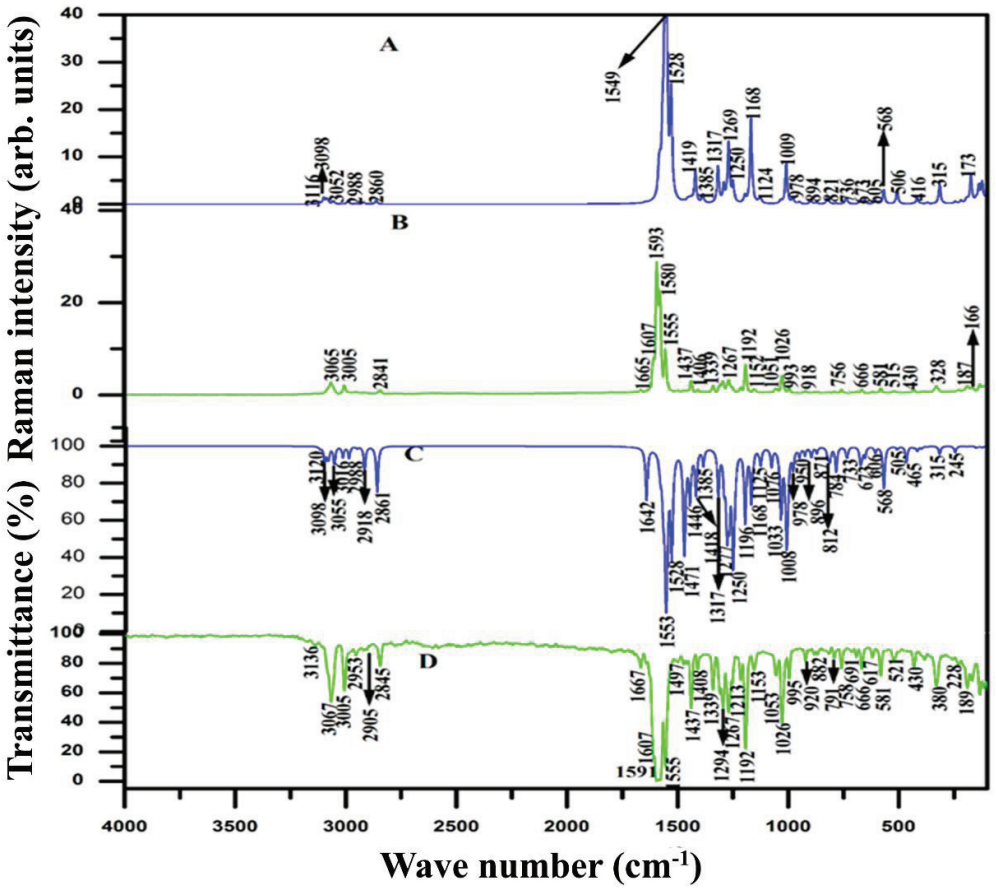

Fig. 7.2 Simulated (C, A) and experimental (D, B) Fourier Transform Infrared and Raman spectra of (2E)-3-(3-Bromo-4methoxyphenyl)-1-(pyridin-2-yl)prop-2-en1-one at Becke three Lee-Yang-Parr /6-31G basis set.**

7.4.1 Phenyl ring vibrations

The C-H stretching vibrations occur in the region 3100-3000 cm^{-1} and the selection rule allows three modes 2,20a, and 20b for the asymmetric tri substituted phenyl ring. The mode 2 of asymmetric tri substituted phenyl ring occurs in the range 3040-3100 cm^{-1}. The strong band at 3067 cm^{-1} in IR and a weak band at 3065 cm^{-1} in Raman has been assigned to CH stretching vibration of phenyl ring. The weak intensity band observed in IR at 3136 cm^{-1} has been assigned to C-H stretching vibration of pyridine ring which is due to the intermolecular interaction of C-H…Br.

This intermolecular interaction causes the shifting of CH stretching vibrations. The calculated wave numbers at 3120 cm^{-1} by DFT method is assigned to C-H stretching vibration of pyridine ring. C-H stretching vibration of the propanone group is observed in IR at 3005 cm^{-1} as a strong band and in Raman at 3005 cm^{-1} as a weak band.

Normal vibration 3, 15 and 18b arises due to CH in-plane bending vibrations of the tri substituted phenyl ring are expected in the range 1300-1000 cm^{-1}. Mode 3 of phenyl ring is observed in IR at 1267 cm^{-1} as a strong band and as a weak band at 1294 cm^{-1} and in Raman as a weak band at 1267 cm^{-1}. The weak band in IR at 1153 cm^{-1} and a weak band in Raman at 1152 cm^{-1} have been assigned to mode 15 of phenyl ring. Selection rule allows five C-C stretching modes 8a, 8b, 19a, 19b and 14 for the phenyl ring which are substituent dependant. The degenerate mode 8a of the asymmetric tri substituted ring is expected in the range 1549-1591 cm^{-1} whereas the mode 8b occurs in the region 1617-1620 cm^{-1}. Mode 8a of phenyl ring C-C stretching is coupled with C-H bending vibration. Bands identified at 1591 cm^{-1} and at 1555 cm^{-1} in IR and Raman bands identified at 1593 cm^{-1}, 1580 cm^{-1} and at 1555 cm^{-1} are the strong bands assigned to this mode. A weak band at 1408 cm^{-1} in IR and 1406 cm^{-1} in Raman has been assigned to C-C stretching vibration of pyridine ring. Mode 19b appears as a weak band in IR at 1497 cm^{-1} which is strongly coupled with C-H bending. The C-N stretching vibrations of pyridine ring is observed in the region 1600 cm^{-1} -1500 cm^{-1}. The strong band observed in IR and Raman at 1555 cm^{-1} and a shoulder band at 1580 cm^{-1} in Raman has been assigned to this mode. The C-N in plane bending vibrations is observed in IR at 521cm^{-1} and in Raman at 515 cm^{-1}.

7.4.2 Methoxy group vibration

In aromatic molecules CH_3 asymmetric stretching vibrations occurs in the range 2970-2920 cm^{-1} and the symmetric vibration occurs in the range 2850-2815 cm^{-1}. IR bands observed at 3005 cm^{-1} ($CH_3$is) 2953 cm^{-1} and 2905 cm^{-1} (CH_3ops) and Raman band at 3005 cm^{-1} ($CH_3$is) have been assigned to asymmetric mode. The symmetric vibration is observed in IR as a strong band at 2845 cm^{-1} (CH_3S) and in Raman at 2841cm^{-1} (CH_3S). Medium band appears at 1153 cm^{-1} in IR spectrum and a weak band occurs at 1152 cm^{-1} in the Raman spectrum has been assigned to CH_3 rocking mode. Strong band appears at IR and Raman at 1437 cm^{-1} has been assigned to CH_3 bending mode.

7.4.3 Carbonyl group vibration

The C=O stretching vibration of the carbonyl group is expected to appear in the range 1715-1680 cm^{-1} [132-135]. The C=O stretch in the carbonyl group depends on the bond strength which in turn depends on the inductive, steric and lone pair of electron on carbon atom. Medium IR and Raman bands at 1667 cm^{-1} and 1665 cm^{-1} respectively corresponds to C_{11}-O_{12} stretching mode. The lowering of stretching wave number of C=O vibration is due to the conjugation of carbonyl group in the phenyl ring. Red shifting of C=O spectral band provides the spectral evidence for the formation of weak intermolecular hydrogen bonding which contributes to the stability of the molecule. Intensification of intensities in infrared bands signifies the conjugation. The C-O in plane bending and out of plane vibrations is expected in the range 725±70 cm^{-1} and 540±80 cm^{-1} respectively [136]. Medium band in IR at 673 cm^{-1} and weak band in Raman at 664 cm^{-1} has been assigned to in plane bending

mode. IR and Raman bands at 581 cm^{-1} has been assigned to out of plane bending vibration.

7.4.4 C-Br Vibration

The C-Br group vibrations assigned by Mooney are in the frequency range 1129-480 cm^{-1}. C-Br stretching mode appears as a medium band in Raman at 329 cm^{-1} and 666 cm^{-1} and in IR as a weak band at 882 cm^{-1} and 691 cm^{-1}. The lowering of C-Br (~151 cm^{-1}) stretching mode provides the spectral evidence for the existence of C-H...Br intermolecular interaction in the title molecule. Weak band observed in Raman at 168 cm^{-1} has been assigned to C-Br bending mode.

Table 7.3: Calculated vibrational wavenumbers, observed IR and Raman frequencies, IR and Raman intensities and their assignments with PED% for PYR

Experimental		ν_{SQM}	I_{IR}	I_{Ra}	Assignment with PED%≥10%)
ν_{IR} (cm^{-1})	ν_{Raman} (cm^{-1})				
3136 w	-	3120	3.316	0.539	ν (CH) ring1 (99)
-	-	3099	22.71	1.53	ν (CH) ring1 (99)
-	-	3086	11.14	1.27	ν (CH) ring2 (99)
-	-	3083	1.107	1.23	ν (CH) ring2 (99)
-	-	3080	11.68	1.11	ν (CH) ring1 (99)
-	-	3056	20.29	0.694	ν (CH) ring1 (99)
3067 s	-	3053	6.066	0.660	ν (CH) ring2 (99)
-	-	3017	15.38	0.150	ν2 (CH) (98)
3005 s	3005 w	2989	16.81	0.804	ν (CH3)is (91)
2953 w	-	2952	2.535	0.221	ν3(CH) (99)
-	-	2918	33.68	0.413	ν (CH3)ops (88)
2845 m	2841 w	2861	72.92	0.845	ν(CH3) (99)
-	-	1642	85.49	0.641	ν(CO)ss (56)+ν (2CC)as (10)
1591 vs	1593 s	1584	3.826	10.1	ν(CC)ring2(45)+δ(CH)ring2 (11)
-	1580 s	1579	26.05	11.7	ν(CC)ring1(41)+ ν(CC)ring2(13)+ ν(CN)ring2(11)+ δ(CH)ring1 (10)

Table 7.3 (cont.)

1555 s	1555 s	1567	69.96	24.4	ν(CC)ring1(47)+ ν(CN)ring1(17)+ δ(CH)ring1 (14)
-	-	1553	565.1	100	ν 2(CC)as(23)+ν1(CO)ss(19)+ ν(CC)ring2(17)
1497 w	-	1528	227.4	25.4	ν(CC)ring2(52)+ δ(CH)ring2 (10)
-	-	1471	221.4	1.09	ν(CC)ring2(30)+ δ(CH)ring2 (30)+ ν1(CO)ss(12)
-	-	1454	4.460	1.56	δ (CHN) ring1(35)+ ν(CN)ring1(20)+ δ(CH)ring1 (17)+ ν(CC)ring1(47)
-	-	1446	82.58	1.68	δ (CH3)ip (82)+(CH3)rock(13)
1438 s	1437 w	1437	6.646	1.87	δ (CH3)op (79)+ ν(CH3)is (14)
1408 w	1406 w	1420	17.02	6.97	δ(CH)ring1 (40)+ ν(CC)ring1(21)+ δ(CH3)sb(14)
-	-	1418	58.651	6.44	δ(CH3)sb(63)
-	-	1385	24.46	2.18	ν(CC)ring2(51)+ δ(CH)ring2 (23)
1339 s	1339 w	1317	71.69	2.18	ν(CC)ring2(37)+2(CH)rock (13)+ ν1(CC)as(12)
1294 w	-	1291	51.51	4.74	ν(CC)ring2(29)+ ν(CC)ring1(21)+ ν(CN)ring1(16)
-	-	1277	152.7	4.65	δ (CHN) ring1(16)+ ν(CC)ring2(15)
-	-	1269	28.75	13.4	ν(CN)ring1(17)+ ν(CC)ring1(29)
1267 w	1267 w	1268	83.18	13.3	3(CH)rock (20)+ δ(CH)ring2 (12)+ δ (CHN) ring1(11)
-	-	1250	259.7	5.17	ν(CC)ring2(52)+1 ν (OC)(30)
1213m	-	1241	25.00	2.03	δ(CH)ring2 (55)+ 3(CH)rock (12)+ ν(CC)ring2(11)
1192 s	1192 m	1196	132.9	2.22	ν1(CC)as(16)+ ν(CC)ring1(12)+ 2(CH)rock (12)+ ν1(CC)as(11)
1153 m	1151 m	1168	88.90	18.3	ν 2 (CC)ss(19)+ δ(CH)ring2 (55)+ δ(CH)ring2 (18)+ ν(CC)ring2(15)+ 2(CH)rock (12)
-	-	1158	7.178	4.32	(CH3)ir (64)+ (CH3)is (11)
-	-	1133	4.498	1.19	δ(CH)ring1 (78)+ ν(CC)ring1(20)
-	-	1125	23.44	1.56	δ(CH)ring2 (44)+ ν(CC)ring2(28)
-	-	1121	0.873	1.12	(CH3)or (79)+(CH3)is (17)
1053 m	1051 m	1076	27.49	0.183	δ(CH)ring1 (46)+ ν(CC)ring1(30)

Table 7.3 (cont.)

1026 s	1026 m	1035	66.56	0.999	ν(CC)ring1(40)+ δ(CH)ring1 (15)+1(OC)s(12)
-	-	1032	61.91	1.11	1(OC)as(35))+ ν(CC)ring2(20)+ ν(CC)ring1(12)
-	-	1009	176.1	8.62	ν(CC)ring1(25)+ ν1 (CC)s(21)+ ν 1 (CC)as(21)
995 m	993 w	1003	54.17	4.01	R_{trgd2}(37) +1(OC)as(35))+ ν(CC)ring2(11)
-	-	981	0.064	1.48	$(CH1)_{wag}$(81)
-	-	979	28.88	1.69	R_{trgd1}(62) + ν(CN)ring1(21)+ ν(CC)ring1(15)
-	-	950	12.47	0.581	$(CH1)_{wag}$(32)+ 3$(CH)_{wag}$(28)+1 $(CH)_{wag}$(11)
-	-	948	1.170	0.542	$(CH1)_{wag}$(62)+ Rat1(16)
920 w	918 w	925	11.63	0.134	$(CH1)_{wag}$(43)+ Rat2(23)+ Rato2 (21)
-	-	902	0.288	0.496	$(CH2)_{wag}$(55)+ Rat2(13)+ Rpk2(10),
-	-	896	14.39	0.880	ν(CC)ring2(24) + 2 (CC) def(15) + 3 (CC) def(15)
882 w	-	896	0.001	0.880	$(CH1)_{wag}$(84)
-	-	872	9.048	0.441	2$(CH)_{wag}$(51)+1$(CO)_{wag}$+ τ(CH)ring2(11)
-	-	822	15.52	1.49	1(CC)s(17)+ Rad2(16)+ ν(CC)ring2(12)
-	-	812	19.18	0.475	$(CH2)_{wag}$(55)+2 $(CO)_{wag}$(18)
791 w	-	784	37.25	0.294	$(CH1)_{wag}$(28)+ Rpk1(23)+$(CC1)_{wag}$(15)
758 w	758 w	739	6.214	1.42	1(OC)s(16)+ Rtd2 (14)+ δ(COC)ring2(12)+ Rad1 (10)
-	-	734	12.50	1.10	$(CH1)_{wag}$(45)+ Rpk1 (39)
-	-	716	0.008	0.167	Rpk2 (42)+ $(CO)_{wag}$(30)
691 w	-	674	23.71	0.980	Rad1 (24)+ Rado2(19)+ δ(COC)ring2(10)
666 w	666 w	667	9.924	0.687	Rpk1(37)+1$(CO)_{wag}$(23)+ $(CH1)_{wag}$(14)
-	-	654	14.88	0.963	Rado2 (44)+ Rad1(15)
617 w	-	607	8.741	0.987	Rado1(75)
-	-	568	5.514	3.07	$(CC2)_{wag}$ (32)+Rato2(24)+$(2CO)_{wag}$ (16)
581 m	581 m	568	59.98	3.07	δ(COC) (36)+ δ(CCO) (18)
521 w	515 w	507	4.139	3.02	1(CC)def(27)+ δ(COC) (14)+ δ(CH)ring1 (12)
-	-	466	22.69	0.125	Rad2(27)+ δ(CCO) (16)+ δ(COC) (10)

Table 7.3 (cont.)

-	-	434	0.444	0.241	Rat2 (46)+ Rato2 (45)
-	-	430	1.463	0.282	Rat2 (41),+Rato2 (36)
430 m	430 w	417	6.463	1.41	δ(COC) (18)+ δ(CCC) (14)+1(CC)as(11)+ Rad1(10)
-	-	397	3.208	0.239	Rato1 (53)+Rat1(44)
-	-	371	0.850	0.414	Rat2(18)+Rato2(17)+2$(CO)_{wag}$ (12)+2$(CC)_{wag}$(11)
-	328 w	316	5.527	4.20	ν(CBr)ring2(19)+δ (CN)ring1(14)+ Rad2 (11)+1COro(10)
-	-	315	5.861	4.29	δ(COC) (51)+(CH3)is(20)+ ν(CBr)ring2(10)
-	-	245	8.832	0.613	(CH3)is+ δ (CN)ring1(17)+ δ(COC) (18)
-	-	218	0.004	0.890	τ(CH3) (38)+ Rat2 (28)+(CH3)is(17)
189 w	-	195	0.389	1.43	(CH3)is(45)+ ν(CC)(10)+(CC)def(10)
-	-	190	0.296	1.53	τ(CH3) (34)+ (CH3)is(31)+ Rat2(16)+ Rato2 (14)
-	166 w	174	0.171	6.11	Rat1(41)+ τ1(CH) (12)+(CC1)wag(10)
-	-	150	2.216	1.91	(CH3)is(52)+ δ(CCO) (15)+ δ(COC) (10)
-	-	138	0.442	4.36	(CH3)is(25)+ Rato2(25)+ τ(CH3) (18)
-	-	123	1.957	4.95	δ(CBr) (26)+1(CC)def(18)+ δ(CCC) (18)+ δ (CN)ring1(16)
-	-	101	0.069	2.42	ν 1(CH3)(18)+ Rato2 (16)+ τ(CO) (15)+ τ1(CH) (13)
-	-	87	7.310	3.24	τ(CH3) (32)+(CH3)is+ τ(CO) (26)
-	-	51	0.363	1.36	(CH3)is (57)+ τ (CH3)(17)
-	-	36	0.580	46.1	(3CC)def (35)+(2CC)def(26)+ δ (CCC2)(16)+CCd1 (12)
-	-	30	1.692	84.2	(CH3)is (53)+ ν (CO)1(20)
-	-	13	2.015	171	(CH3)is (60)+1 ν (CH3)(19)

ν_{IR}- Frequency of Infrared

ν_{Raman}- Frequency of Raman

ν_{SQM} –Scaled frequency

I_{IR}- Infrared intensity

I_{Ra}- Raman intensity

PED- Potential energy distribution

Abbreviation used: vs: very strong; s: strong; m: medium; w: weak. ν: stretching; δ: bending; as: asymmetric stretching; ss: symmetric stretching; op:out of plane stretching; ip: inplane stretching; sb: symmetric bending ; pb: out of plane bending; ib: inplane bending ; rock: rocking; opr: out of plane rocking; ir: in plane rocking; trgd: trigonal deformation; wag; wagging; puck: puckering; ast: assymtortic torsion; asd: assymtotic deformation; asdo: assymtotic deformation outplane; τ: torsion.

7.5 UV-VISIBLE ANALYSIS

TD-DFT method is the most popular method to treat the excited states of electronic structure that are caused by the interaction of light. It also explains the optical properties of large compounds. The gas phase and the solvent phase UV-Visible spectrum are obtained at CAM-B3LYP method. Experimental spectra are recorded in the range 215 nm-1980 nm. Table 7.4 describes the intense wavelength, oscillator strength, and the experimental wavelength. Gas phase shows an intense peak at 290 nm with oscillator strength of 0.8102 and the solvent phase displays an intense peak at 299 nm with oscillator strength of 0.9114. The experimental bands observed at 266 nm corresponds to π-π* transition.

Table 7.4: Experimental and calculated absorption wavelengths, energies and oscillator strengths of PYR using TD-DFT method at CAM B3LYP level

Excitation	CI expansion coefficient	Wavelength (nm) calc.gas phase CAM-B3LYP	Oscillator strength (f)	Experimental (nm)
Excited state 1	Singlet A			
75-81	0.16270			
78-81	0.65701	352	0.0001	
78-86	-0.13604			
Excited state 2				
74-81	-0.12610			
80-81	0.66239	290	0.8102	266
80-83	-0.10068			
Excited state 3	Singlet A			
79-81	0.45867			
79-82	-0.16485			
79-83	-0.16181	255	0.0247	
80-83	-0.13810			
80-84	0.41416			

Excitation	CI expansion coefficient	Wavelength(nm) calc.ethanol CAM-B3LYP	Oscillator strength (f)	Experimental (nm)
Excited state 1	**Singlet A**			
75-81	0.20130			
78-81	0.64538	344	0.0001	
78-86	0.11944			
Excited state 2	Singlet A			
76-81	-0.12808			
80-81	0.66275	299	0.9411	266
80-82	0.10701			
Excited state 3	Singlet A			
79-81 79-82	0.47010 0.17527			
79-83	0.11944	255	0.0225	
79-84	0.12053			
80-83	0.22502			
80-84	-0.36585			

7.6 OPTICAL ENERGY GAP DETERMINATION

Measurement of optical transmittance provides a satisfactory way to determine the absorption edge and hence the energy band gap. The ability of a material to absorb photons of a given wavelength is measured quantitatively by the optical absorption coefficient (α), measured in units of reciprocal distance. There are two major types of intrinsic absorption processes involved in determining α, they are the direct and indirect absorption. In the high absorption region, the absorption coefficient (α) is related to the photon energy according to the following relation [137,138].

$$\alpha h\upsilon = A\left(h\upsilon - E_g^{opt}\right)^p$$

where, 'h' is Planck constant, 'ν' is the frequency, 'A' is an energy independent constant (it is a parameter which depends on the transition probability), 'E_g^{opt}' is the optical energy gap of the molecule. As a general rule, the larger the band gap, the smaller is the value of 'α' for a given wavelength but absorption coefficient also depends on the density of states in the conduction and valence bands. Usually the plot of $(\alpha h\upsilon)^2$ or $(\alpha h\upsilon)^{1/2}$ against (hυ) provides the nature and optical band gap value of a molecule. At the absorption edge, α rises abruptly reaching values of 10^5 cm^{-1} and beyond the absorption edge, decreases and the edge shift towards shorter λ. The band gap of the molecule can be deduced from the extrapolation of the linear part of the graph relative to the function $(\alpha h\nu)^2 = f(h\nu)$. A typical plot drawn between 'hυ' and '$(\alpha h\upsilon)^2$' along with the experimental UV is presented in Fig. 7. 3. The optical band gap of the sample can be determined from modified plot according to Tauc. Obtained optical band gap value is 3.96 eV. The decrease in value of energy gap increases the stability.

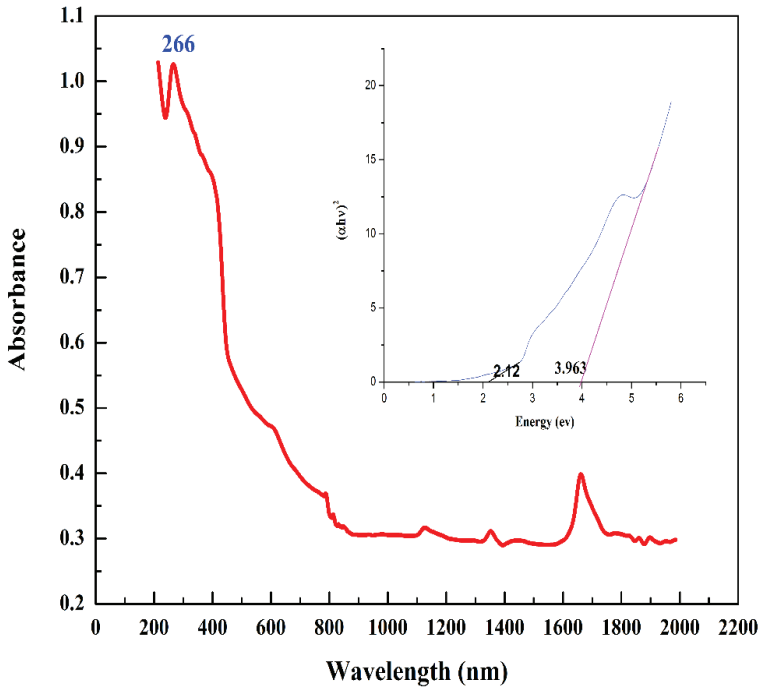

Fig. 7.3 Tauc plot of PYR

7.7 HOMO-LUMO ANALYSIS

The magnitude of the HOMO-LUMO gap has very important chemical implications, even if qualitatively evaluated. A large gap implies good thermodynamic stability of the compound, whereas a small gap suggests an easy electronic transition. The energy difference between the HOMO and LUMO is termed the HOMO–LUMO gap. HOMO and LUMO are sometimes called frontier orbital's in frontier molecular orbital theory.

HOMO which can be thought as the outermost orbital containing electrons that has the ability to donate electron and LUMO can be thought as the innermost

orbital containing free places to accept electrons. The eigen values of HOMO and LUMO and their energy gap replicate the chemical activity of the molecule. An electronic system with a larger HOMO-LUMO gap should be less reactive than one having a smaller gap [139]. The 3-D plots of the HOMO and LUMO for the PYR is shown in Fig. 7. 4. LUMO orbital lies mainly on the phenyl ring and the pyridine ring while HOMO orbital is located on the phenyl ring and the bridge. The HOMO-LUMO transition implies an electron density transfer to the phenyl and pyridine ring along the bridge. The HOMO energies, the LUMO energies and the energy gap for PYR molecules have been calculated using B3LYP level with 6-31G** basis set. The electronic energy gap determined by means of HOMO-LUMO is -0.143 eV. The decrease in energy gap indicates low stability and high reactivity of the molecule.

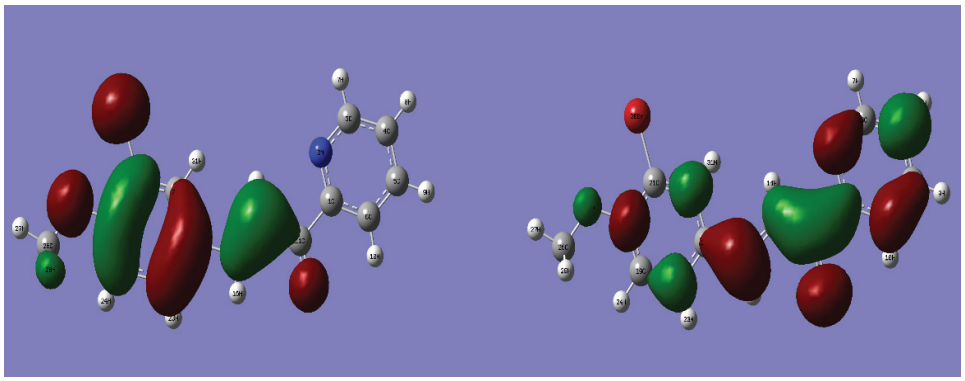

Fig. 7.4 HOMO-LUMO PLOT OF PYR

7.8 CONCLUSION

Using DFT method the molecular structure was modeled and it agrees well with the experimental structure. Scaled quantum mechanical calculations were performed using non-redundant natural coordinates to carry out authentic vibrational assignments. The recorded FT-IR and FT-Raman spectral outcome were compared with the computed values. The experimentally observed FT-IR and FT-Raman spectra show a good correspondence with the computed values. Blue shifting of (36 cm^{-1}) C-H stretching mode provides the spectral substantiation for the intermolecular interactions of C-H...Br. The lowering of stretching wave number of C=O vibration is due to the conjugation of carbonyl group in the phenyl ring. Red shifting of C=O (20 cm^{-1}) spectral band provides the spectral evidence for the formation of weak intermolecular hydrogen bonding which contributes to the stability of the molecule. Transfer of electron charge from π antibonding of C=O to the σ antibonding of C=O causes weakening of the bond and its elongation. The optical band gap energy of the studied molecule is 3.96 eV whereas the electronic band gap energy obtained using Homo-Lumo is -0.143 eV. Low value of HOMO-LUMO energy gap demonstrates an increasing level of biological activity.